



DR. MARIZE VALADARES (Orcid ID : 0000-0002-0379-1325)

Article type : Research Article

LQFM184: A Novel Wide Ultraviolet Radiation Range Absorber Compound

Daniela C. Vinhal¹, Renato Ivan de Ávila², Thaisângela L. Rodrigues², Andressa K. Silva³, Larissa C. Moreira², Marize C. Valadares^{2*}, Rangel M. Luzin³, Luciano M. Lião³, Eric de S. Gil⁴, Boniek G. Vaz⁵, Rogério J. Assis⁶, Pablo J. Gonçalves⁶, Vera Isaac⁷, Luiz C. da Cunha¹, Ricardo Menegatti^{8*}

¹Núcleo de Estudos e Pesquisas Tóxico-Farmacológicas (NEPET), Faculdade de Farmácia, Universidade Federal de Goiás, Goiânia, GO, Brazil.

²Laboratório de Ensino e Pesquisa em Toxicologia In Vitro (Tox In), Faculdade de Farmácia, Universidade Federal de Goiás, Goiânia, GO, Brazil.

³Laboratório de Ressonância Magnética Nuclear, Instituto de Química, Universidade Federal de Goiás, Goiânia, GO, Brazil.

⁴Faculdade de Farmácia, Universidade Federal de Goiás, Goiânia, GO, Brazil.

⁵Laboratório de Cromatografia e Espectrometria de Massas, Universidade Federal de Goiás, Goiânia, GO, Brazil.

This article has been accepted for publication and undergone full peer review but has not been through the copyediting, typesetting, pagination and proofreading process, which may lead to differences between this version and the [Version of Record](#). Please cite this article as [doi: 10.1111/php.13349](https://doi.org/10.1111/php.13349)

This article is protected by copyright. All rights reserved

⁶Instituto de Física, Universidade Federal de Goiás, Goiânia, GO, Brazil.

⁷Laboratório de Cosmetologia (LaCos), Departamento de Fármacos e Medicamentos, Faculdade de Ciências Farmacêuticas, Universidade Estadual Paulista Júlio de Mesquita Filho, Araraquara, SP, Brazil.

⁸Laboratório de Química Farmacêutica Medicinal (LQFM), Faculdade de Farmácia, Universidade Federal de Goiás, Goiânia, GO, Brazil.

*Corresponding authors email: rm_rj@yahoo.com, (Ricardo Menegatti) marizecv@ufg.br
(Marize C. Valadares)

ABSTRACT

The use of sunscreen has become an indispensable daily routine since UV radiation is a critical environmental stress factor for human skin. This study focused on the design, synthesis, thermal/chemical stability and efficacy/safety evaluations of a new heterocyclic derivative, namely LQFM184, as a photoprotective agent. The compound showed stability when submitted under oxidative and high temperature conditions. It also revealed an absorption at 260-340 nm (UVA/UVB), with a main band at 298 nm and a shoulder close to 334 nm. LQFM184 showed capacity to interact with other existing UV filters, promoting an increase in the sun protection factor. In relation to acute toxicity, its estimated LD₅₀ was > 300-2000 mg/kg, probably with a low potential of inducing acute oral systemic toxicity hazard. In addition, our data showed that this compound did not have eye irritation, skin sensitization or phototoxicity potentials. Taken together, these findings make LQFM184 a promising ingredient to be used, alone or in association with other UV filters, in cosmetic products such as sunscreens with a broad-spectrum of protection.

Keywords: Heterocyclic derivative; Photoprotection; Sunscreen; Green chemistry; UV filter.

INTRODUCTION

Solar ultraviolet radiation (UVR), mainly consisted of UVA (320-400 nm) and UVB (290-320 nm), achieves the Earth's surface and can promote beneficial effects to human skin health, such as induction of vitamin D production [1-3]. However, excessive sun exposure can also trigger several harmful clinical consequences, including skin photodamage (e.g. sunburn, premature skin aging), immunosuppression and malignant melanoma [1, 2]. These effects have been increased along with the depletion of the ozone layer and outdoor lifestyle changes [4, 5]. Concerns regarding UVR exposure promoted the development of photoprotective cosmetic products, whose sunscreens have been used as the first choice for protection against excessive solar exposure-induced skin damages [1, 2].

UV filters are classified as organic (e.g. octyl methoxycinnamate, benophenone-3, octocrylene) or inorganic (e.g. zinc oxide, titanium dioxide), based on their composition and mechanism of action [1, 2]. Combination of sunscreen filters is commonly used for increasing the broad-spectrum of protection of the photoprotective cosmetic products [1].

It has been documented in the literature that some sunscreen agents, such as benzophenones (BPs), are able to penetrate the skin and trigger toxicity [6]. Vela-Soria and co-workers developed a method for identifying the presence of BPs in 16 placental tissue samples [7]. To overcome this issue, new agents have been developed, such as bis-ethylhexyloxyphenol methoxyphenyl triazine (BEMT) and methylene bis-benzotriazolyl tetra methyl butyl phenol (MBBT). New sunscreens are considered ideal when are designed to show broad-spectrum, increased photostability, innocuity and solubility in cosmetic oils, with reduced capacity to overcome the skin barriers as well as with minimal toxicological effects, in particular to skin and eyes [8-11]. In this sense, we previously demonstrated that the new molecule LQFM048 showed useful photoprotective and antioxidant properties for the development of a new sunscreen product without potential adverse effects related to eye irritation and skin allergy, for instance [12, 13].

Given the above, this study focused on the design, synthesis, thermal/chemical stability and efficacy evaluations of a new heterocyclic derivative, namely LQFM184 (**2**) [(2,4,6-tris ((E)-2-cyano-3-(4-hydroxy-3-methoxyphenyl)acrylamide)-1,3,5-triazine)] (Fig. 1), to be used as a potential new photoprotective agent in cosmetic products. This compound was originally designed through bioisosterism of functional group strategy, via green chemistry synthetic approach, using the LQFM048 (**1**) as lead compound [12]. In addition, acute toxicological endpoints were investigated to establish the toxicity profile of LQFM184 (**2**).

<Figure 1>

MATERIALS AND METHODS

Chemicals

Tetrahydrofuran (THF) was purchased from Tedia Brazil (Rio de Janeiro, RJ, Brazil). Vanillin, malonolitrine, cianeacetamide, 2,4,6-trichloro-1,3,5-triazine and morpholine were obtained from Acros Organics (Geel, Belgium). Deuterated chloroform (CDCl_3) was acquired from Cambridge Isotope Laboratories Inc (Tewksbury, MA, USA). Methanol, ethyl acetate, ethanol, dimethyl sulfoxide (DMSO), chloroform, dichloromethane, acetic acid, hydrochloric acid (HCl), sodium chloride (NaCl), dichloromethane, hexane and calcium chloride (CaCl_2), potassium phosphate and acetate were acquired from Vetec (Rio de Janeiro, RJ, Brazil), whereas ethylhexyl methoxycinnamate, silica gel 7 60 and vanillin from Merck (Darmstadt, HE, Germany). Tinosorb[®] S was acquired from BASF (Ludwigshafen, Germany). Potassium carbonate (K_2CO_3) was purchased from Synth (SP, Brazil). Graphite was purchased from Metrohm Autolab B.V. (Kanaalweg, Utrecht, The Netherlands), whereas mineral oil was acquired from Biolub Chemistry LTDA (Sorocaba, SP, Brazil). Analytical grade methanol was supplied by J. T. Baker (Phillipsburg, NJ, USA). All electrolyte solutions were prepared using analytical grade reagents and double distilled water. Sodium fluorescein, benzalkonium chloride, Hanks' balanced salt solution (HBSS), Eagle's Minimum Essential Medium (EMEM) with or without phenol red, Dulbecco's modified Eagle's medium (DMEM), fetal bovine serum (FBS), Roswell Park Memorial Institute (RPMI)-1640 medium, HEPES, sodium bicarbonate,

penicillin, streptomycin, amiodarone HCL, *p*-phenylenediamine (PPD), 1-chloro-2,4-dinitrobenzene (DNCB), protease inhibitor cocktail, 3-[4,5-dimethylthiazol-2-yl]-2,5-diphenyl tetrazolium bromide (MTT), propidium iodide (PI), neural red, bicinchoninic acid protein assay kit and bovine serum albumin were acquired from Sigma-Aldrich (St. Louis, MO, USA). Triton X-100 was obtained from Amresco (OH, USA). Human IL-18 Platinum ELISA was purchased from eBioscience (Vienna, Austria), whereas BD OptEIA™ human IL-8 ELISA set kit, FITC-conjugated anti-human CD86 (FUN-1) monoclonal antibody and FITC-isotype control IgG1 (MOPC-21) were acquired from BD Biosciences (San Jose, CA, USA). TRIZOL® reagent was obtained from Invitrogen (Grand Island, NY, USA). SsoAdvanced™ Universal SYBR® Green Supermix and iScript™ gDNA Clear Synthesis kit were acquired from Bio-Rad (Hercules, CA, USA).

General

The ¹H and ¹³C NMR experiments were performed at 25 °C using a Bruker Avance III 500 spectrometer operating at 11.75 T, observing ¹H at 500.13 MHz. The spectrometer was equipped with a 5 mm inverse detection four-channel (¹H, ²H, ¹³C and X-nucleus) TBI probe. For each analysis, 20 mg of sample were dissolved in 500 μL of DMSO-d₆ and tetramethylsilane (TMS) as the internal standard. The mass data were obtained using a QTOF Micro mass spectrometer equipped with an ESI source (Waters, Manchester, UK). The parameters of the mass spectrometer used were the following: nebulization gas (500 L/h) at 140°C, cone gas set to 50 L/h, and source temperature set to 100°C. Capillary and cone voltage were set to 4500 V and 25 V, respectively. QTOF acquisition rate was set to 1.0 s, with a 0.4 s inter-scan delay and the data processed on MassLynx 4.0 software (Waters, Manchester, UK). Analytes were acquired using LockSpray and phosphoric acid (0.1% in acetonitrile/water, 1:1) as internal standard to ensure accuracy mass. The analyses were performed by direct infusion with a syringe pump at 5.0 μL/min flow ratio. Infrared spectra were acquired using a Nicolet-55a Magna spectrophotometer (GMI, MN, USA) with potassium bromide plates.

Synthesis

Synthesis of 2-(4-hydroxy-3-methoxybenzylidene)malononitrile (5) [13]

Vanillin (**3**) (500 mg, 3.30 mmol) and malononitrine (**4**) (218 mg, 3.30 mmol) were diluted in water (5 mL) at room temperature. Morpholine (5 mol %) was then added to reaction, by agitation for 1 h. The residue was divided between water and CH₂Cl₂, the phases were separated and the aqueous layer was extracted into 3 x 15 mL with CH₂Cl₂. The organic layers were dried (Na₂SO₄), concentrated *in vacuo*, and the rough product used without any purification. The derivative (**5**) (607 mg, 92%) was obtained as a yellow solid, mp 131°C, R_f = 0.90 CH₂Cl₂: MeOH (95:5, v/v); IR max (KBr) cm⁻¹: 3400-3300 (ν O-H), 2951 (ν C-H), 2236 (ν CN) and 2220 (ν CN) (Figure. S1, Supporting Information); RMN ¹H (500 MHz) DMSO-d₆ (δ): 10.82 (1H, s, OH); 8.27 (1H, s, H-3); 7.63 (1H, d, *J* = 2.10 Hz, H-2'); 7.50 (1H, dd, *J* = 2.10 and 8.40 Hz, H-6'); 6.98 (1H, d, *J* = 8.40 Hz, H-5'); 3.81 (3H, s, OCH₃) (Figure S2 and Table S1, Supporting Information); ¹³C (125 MHz) DMSO-d₆ (δ): 160.6 (1C, C-3); 153.7 (1C, C-4'); 147.8 (1C, C-3'); 127.7 (1C, C-6'); 123.1 (1C, C-1'); 116.2 (1C, C-5'); 115.2 (2C, C-1 and 4); 113.1 (1C, C-2'); 74.8 (1C, C-2); 55.5 (1C, OCH₃) (Figures S3, S4 and Table S1, Supporting Information); [M-H]⁻ *m/z* of 199.05122 (Figure S5, Supporting Information).

Synthesis of (E)-2-cyano-3-(4-hydroxy-3-methoxyphenyl)acrylamide (6) [14]

2-(4-hydroxy-3-methoxybenzylidene) malononitrile (**5**) (1.0 mmol, 200 mg) and Cu(OAc)₂·H₂O (20 mg, 0.1 mmol) H₂O (0.2 mL) in HOAc (10.0 mL) were stirred for 7 h at 80°C. Then, the mixture was separated in water and CH₂Cl₂, the phases were divided and the aqueous layer was extracted into 3 x 15 mL with CH₂Cl₂. The organic layers were then dried (Na₂SO₄), concentrated *in vacuo* and the mixture was used without additional steps. The resulting product (**6**) (202 mg, 93%) was a yellow solid, mp 205°C, R_f = 0.50 CH₂Cl₂: MeOH (95:5, v/v) (7:3, v/v); IR max (KBr) cm⁻¹: 3474 (ν N-H), 3300 (ν N-H), 2211 (ν CN) and 1683 (ν C=O) (Figure S6, Supporting Information); RMN ¹H (500 MHz) DMSO-d₆ (δ): 10.26 (1H, s, H-4'); 8.06 (1H, s, H-3); 7.66 (1H, d, *J* = 2.10 Hz, H-2'); 7.46 (1H, dd, *J* = 2.10 and 8.40 Hz, H-6'); 6.94 (1H, d, *J* = 8.40 Hz, H-5'); 3.81 (3H, s, OCH₃) (Figure S7 and Table S2, Supporting Information); ¹³C (125 MHz) DMSO-d₆ (δ): 163.2 (1C, C-1); 151.2 (1C, C-4'); 150.7 (1C, C-3); 147.7 (1C, C-3'); 125.8 (1C, C-6'); 123.2 (1C, C-1'); 117.3 (1C, C-4); 115.9 (1C, C-5'); 113.1 (1C, C-2'); 101.5 (1C, C-2); 55.2 (1C, OCH₃) (Figures S8, S9 and Table S2, Supporting Information); [M-H]⁻ *m/z* of 217.06177 (Figure S10, Supporting Information).

Synthesis of (E)-2-cyano-3-(4-hydroxy-3-methoxyphenyl)acrylamide (6) [15]

Vanillin (**3**) (152 mg, 1.00 mmol) and cyanoacetamide (**7**) (84 mg, 1.00 mmol) were mixed for 1 h at 75 °C. After, 20 mL of water was added and the formed precipitate was filtered off under vacuum. The derivative material (**6**) (174 mg, 80%) was used without rather purification and showed the following parameters: yellow solid, mp 205°C, Rf = 0.50 CH₂Cl₂: MeOH (95:5, v/v) (7:3, v/v).

Synthesis of 2,4,6-tris ((E)-2-cyano-3-(4-hydroxy-3-methoxyphenyl)acrylamide)-1,3,5-triazine (2) [16, 17]

(E)-ethyl 2-cyano-3-(4hydroxy-3-methoxyphenyl)acrylate (**6**) (763 mg, 3.50 mmol), Na₂CO₃ (370 mg, 3.50 mmol), 2,4,6-trichloro-1,3,5-triazine (**8**) (184 mg, 1.00 mmol) and acetonitrile (5.0 mL) were mixed at 80°C for 24 h to obtain a heterogeneous mixture. The mixture was split in aqueous and organic phases (CH₂Cl₂). Then, the aqueous layer was extracted with CH₂Cl₂ and the combined organic layers were dried (Na₂SO₄) and concentrated using *vacuo*. The crude product was solubilized in 5.0 mL of DMF and poured into 50.0 mL of AcOH/H₂O (1:9, v/v). LQFM184 (**2**) (452 mg, 62%) was obtained as a beige solid, mp 147° C, Rf = 0.20 CH₂Cl₂: MeOH (95:5, v/v); IR max (KBr) cm⁻¹: 3290 (ν N-H), 3275 (ν N-H), 2937 (ν C-H) and 1692 (ν C=O) (Figure S11, Supporting Information); RMN ¹H(500 MHz) DMSO-d₆ (δ): 8.19 (1H, *s*, H-3); 7.71 (1H, *d*, *J* = 1.90 Hz, H-2'); 7.57 (1H, *dd*, *J* = 1.90 and 8.40 Hz, H-6'); 7.43 (1H, *d*, *J* = 8.40 Hz, H-5'); 3.79 (3H, *s*, OCH₃) (Figure S12 and Table S3, Supporting Information); ¹³C (125 MHz) DMSO-d₆ (δ): 172.8 (3C, C-2''); 162.5 (1C, C-1); 150.8 (1C, C-3'); 149.9 (1C, C-3); 142.4 (1C, C-4'); 131.2 (1C, C-1'); 123.2 (1C, C-5'); 123.1 (1C, C-6'); 116.5 (1C, C-4); 114.3 (1C, C-2'); 106.9 (1C, C-2); 56.0 (1C, OCH₃) (Figures S13, S14, 15 and Table S3, Supporting Information); [M+H]⁺ *m/z* of 730.20082 (Figure S16, Supporting Information).

Cyclic voltammetry analysis

Voltammetric analyses of the LQFM184 (**2**) were made using a potentiostat/galvanostat (μAutolab III®), controlled by the GPES 4.9® software (Eco-Chemie, Utrecht, The Netherlands). The electrodes consisted of a carbon paste working electrode, a Pt wire counter electrode and an Ag/AgCl/KCl 3M as the reference electrode. Pulse amplitude (50 mV) and width (0.5 s), associated with a scan rate 10 mV

s⁻¹, were set up for differential pulse voltammetry (DPV). The experiments were performed in triplicate using a one-compartment electrochemical cell.

Thermogravimetric analysis

Regarding thermal stability of LQFM184 (**2**), it was evaluated using a DTG-60H thermobalance (Shimadzu, MD, USA). A sample of the compound (4 mg) was evaluated by heating process from 30 to 600°C (flow rate of 50 mL min⁻¹ and a heating rate of 10°C/min) under synthetic air atmosphere.

Photophysical characterization

Photophysical data of LQFM184 (**2**) were obtained through UV-Vis spectra, obtained in a double beam spectrophotometer model U-2900 (Hitachi High-Technologies, Tokyo, Japan). The fluorescence spectra were obtained using a fluorescence spectrophotometer F-7000 (Hitachi High-Technologies).

Evaluation of Sun Protection Factor (SPF)

For SPF determination, O/W emulsions containing LQFM184 (**2**) were prepared [18]. The measurements of the SPF were made using Optometrics SPF 290S (Laser Components, Olching, Germany) following the protocol recommended by the manufacturer [19, 20]. In Transpore[®] tapes (50 cm²) (3M, MN, USA) placed directly on the support, 110 mg of the sample were applied, forming a uniform film of 2 mg/cm². After application, the tapes with the samples were dried for 15 min. The support was then introduced directly into the equipment, and the readings were performed by the emission of ultraviolet radiation generated through a xenon lamp with a wavelength in the range of 290 to 400nm.

***In vitro* toxicological assessment**

Cell cultures

Cell lineages (Balb/c 3T3-A31 fibroblasts, HaCaT human immortalized keratinocytes, SIRC rabbit corneal and U937 human histiocytic lymphoma cells) used in this work were purchased from the Rio de Janeiro Cell Bank (Rio de Janeiro, RJ, Brazil). 3T3, HaCaT or SIRC cells were cultured in complete DMEM and the U937 cells were cultured in RPMI medium. In addition, cell medium was

supplemented with 10% (v/v) heat-inactivated FBS, HEPES (4.5 mM), sodium bicarbonate (170 mM), penicillin (100 IU/mL) and streptomycin (100 mg/mL) under controlled conditions (humidified atmosphere of 5% CO₂ in air at 37°C).

Estimation of acute systemic toxicity: lethal dose (LD₅₀)

The investigation of the acute toxicity potential of LQFM184 (**2**) was performed by the estimation of LD₅₀ through 3T3 neutral red uptake (NRU) assay, according to the protocol prior described by Borenfreund and Puerner [21] and modified by ICCVAM [22]. 3T3 cells were seeded in 96-well plates at 0.5×10^5 cells/mL. After that, cells were exposed to LQFM184 (**2**) (1.6-200 µg/mL) or its vehicle (DMSO 0.4%, v/v) for 48 h of incubation. Then, 100 µL/well of NR (0.25 mg/mL), diluted in DMEM containing FBS (5%, v/v), was added and incubated for 3 h. Cells were then washed with pre-warmed PBS and NR desorb (50 ethanol: 1 acetic acid: 49 ultrapure water) added in each well. Absorbance was measured at 550 nm (Multiskan Spectrum spectrophotometer, Thermo Scientific, Waltham, MA, USA). Cell viability was expressed as a percentage of the control and IC₅₀ value (concentration that inhibited cell growth by 50% compared to untreated group) was calculated. The LD₅₀ was then estimated using the model equation [$\text{Log}(\text{LD}_{50}) = 0.545 \times \log(\text{IC}_{50}, \text{mM}) + 0.757$] [23]. The probable acute oral systemic toxicity classification of LQFM184 (**2**) was then done based on the estimated LD₅₀ and in accordance with the United Nations Globally Harmonized System of Classification and Labeling of Chemicals (UN GSH) [24].

Short time exposure (STE) assay

The STE assay was conducted according to the OECD test guideline N° 491 [25]. Briefly, SIRC cells were seeded in plates at 3×10^3 cells/well followed by 5-day incubation. After that, cells were then exposed to LQFM184 (**2**) (at 5 or 0.05%, w/v) for 5 min at room temperature or exposed to saline, LQFM184 vehicle (5% DMSO in saline) or benzalkonium chloride (at 5 and 0.05%, w/v) diluted in saline. Then, after washing the cells, MTT solution (200 µL/well at 0.5 mg/mL) was added. After additional 2 h incubation, the formazan formed was extracted using DMSO (200 µL/well).

Absorbance was measured at 560 nm. Eye irritation or serious eye damage of the exposure groups was classified in UN GHS categories according to cell viability values for concentrations at 5 and 0.05% of each test material as follows: “no category”, i.e. not classified for eye irritation or serious eye damage if cell viability was $> 70\%$ at 5% and 0.05% concentrations; “category 1”, i.e. serious eye damage when 5% and 0.05% concentrations triggered a cell viability of $\leq 70\%$; or “no prediction can be made” if cell viability for 5% and 0.05% concentrations were $\leq 70\%$ and $> 70\%$, respectively.

Bovine corneal opacity and permeability (BCOP) assay and corneal histomorphometric evaluation

The BCOP assay was performed according to the OECD test guideline N° 437 [26]. Bovine eyes were kindly donated by a local slaughterhouse (Vale do Cedro, Inhumas, GO, Brazil). In brief, excised corneas were put on holders and the two cavities were filled with medium followed by 1 h incubation at 32°C. Then, the medium was renewed to measure the corneal opacity using an OP-KIT Electro Design Opacitometer (Riom, France). Corneas with opacity < 7 were then exposed to the test material for 10 min: PBS (negative control group), benzalkonium chloride (5% w/v in PBS, as positive control), LQFM184 (**2**) (5% w/v in PBS) or its vehicle (5% w/v DMSO in PBS). Corneal epithelium was then washed with medium and the anterior chambers refilled with phenol red-free EMEM, and final opacity values were obtained to calculate corneal opacity. The medium was discarded after incubation followed by refilling of posterior and anterior chambers with medium and fluorescein solution (1 mL at 4 mg/mL in PBS), respectively, for 90 min. Aliquots (200 μ L) from posterior chambers were collected and the absorbance determined at 490 nm. Thus, the permeability values were obtained for each cornea. The following equation was used to calculate “*In Vitro Irritancy Score*” (IVIS): $IVIS = \text{opacity} + (15 \times \text{permeability})$. The corneal irritancy levels of exposure groups were determined based on the obtained IVIS values as follows: “No Category” ($IVIS \leq 3$); “No Prediction Can Be Made” ($3 < IVIS \leq 55$); or “Category 1” ($IVIS > 55$).

Corneas were kept in 10% phosphate buffered formalin and histomorphometric evaluation was performed based on protocol described by Oliveira, Ducas, Teixeira, Batista, Oliveira and Valadares [27]. The tissue sections were observed by a light microscope and photographed using an AxioCamMRc Carl Zeiss camera and analyzed in AxioVs40 V 4.7.2.0 Carl Zeiss software (Axio Scope A1 Carl Zeiss, Jena, TH, Germany). For histomorphometric assessment, about 10 locations in

the central field of the tissue sections were randomly chosen and the measurements of thickness of the epithelium and stroma were conducted.

HaCaT keratinocytes-associated IL-18 assay

IL-18 production by HaCaT cells after exposure to LQFM184 (**2**) was performed in accordance with the protocol described by Corsini et al. [28]. The cytotoxicity evaluation of LQFM184 (**2**) was prior conducted, by seeding 1.5×10^5 cells/mL in a 96 well plate and exposing to LQFM184 (**2**) (1.6-200 $\mu\text{g/mL}$) or its vehicle (0.4% DMSO in complete medium) for 24 h. Then, the MTT assay was performed as described above. Cell viability was expressed as a percentage of the control and IC_{20} value was calculated to perform IL-18 production analysis. Keratinocytes (1.5×10^5 cells/mL) were seeded overnight in a 24-well flat plate and were exposed to non-cytotoxic concentration of LQFM184 (**2**) ($\text{IC}_{20} = 8 \mu\text{g/mL}$), skin sensitizer PPD (40 $\mu\text{g/mL}$), vehicle control (0.4% DMSO) or complete medium only (control cells) for 24 h. Cell lysates were obtained and IL-18 levels of each sample were quantified using Human IL-18 Platinum ELISA (eBioscience) in accordance with the manufacturer's instructions. The protein content of each sample was measured using bicinchoninic acid protein assay kit (Sigma-Aldrich). IL-18 levels data (pg) are expressed based on total intracellular protein content (mg) and stimulation index (SI) was calculated according to the equation: $\text{SI} = \text{IL-18 in treated cells} / \text{IL-18 in vehicle-treated cells}$. Those samples with $\text{SI} \geq 1.2$ associated with a significant IL-18 increase were classified as contact allergens.

Gene expression assay

HaCaT cells were seeded at 1.5×10^5 cells/mL in a 24-well plate and exposed to LQFM184 (**2**) (8 $\mu\text{g/mL}$), PPD (40 $\mu\text{g/mL}$) or vehicle (0.4% DMSO/medium) for 4 h. Then, total RNA was obtained using Trizol[®] (Invitrogen), according to manufacturer's instructions. The integrity of the RNA was evaluated at 260 nm using Nanodrop 2000 spectrophotometer (Thermo Fisher Scientific, Waltham, MA, USA). cDNA samples were prepared using a recombinant reverse transcription kit (iScript[™] gDNA Clear Synthesis kit, Bio-Rad). Quantitative real-time PCR reactions were then performed using SsoAdvanced[™] Universal SYBR[®] Green Supermix kit (Bio-Rad). The *HPTR1* was used as reference

gene and fold change was calculated by DDCT method. Primers are presented in Table 1. The data were calculated as average log₂-fold change in three independent biological replicates ± SD.

<Table 1 >

U937 cell line activation test (U-SENS™) and IL-8 levels analysis

U-SENS™ was performed according to OECD test guideline N° 442E [29]. First, cytotoxicity potential of LQFM184 (**2**) in U937 cells was performed using PI staining in accordance with the guideline to determine LQFM184 (**2**) concentrations that promote viability ≥ 70% (CV₇₀). In a second step, CD86 expression was evaluated by exposing U937 cells to LQFM184 (**2**) (1.25-10 µg/mL), skin sensitizer DNCB (1 µg/mL), vehicle control (0.4% DMSO) or medium only for 45 h. Subsequently, supernatants were collected to determine IL-8 levels using BD OptEIA™ human IL-8 ELISA set kit (BD Bioscience), and cells were washed with PBS + 5% FBS (v/v) and incubated for 30 min at 4°C with staining solution containing buffer and FITC-conjugated anti-human CD86 monoclonal antibody or FITC-isotype control IgG1. After that, cells were washed and stained with PI (3 µg/mL) and analyzed using flow cytometer. Data were calculated as stimulation index (SI) according to the following equation: $SI = [(\%CD86_{\text{treated}} - \% \text{ isotype IgG1}_{\text{treated}}) / (\%CD86_{\text{control}} - \% \text{ isotype IgG1}_{\text{control}})] \times 100$. A positive response for skin sensitization was considered when $SI \geq 150\%$. Regarding IL-8 assay, the same prediction model described in HaCaT keratinocytes-associated IL-18 assay was applied to classify each test material as non-sensitizer or sensitizer.

Phototoxicity evaluation

The phototoxicity potential of the LQFM184 (**2**) was investigated in accordance to the OECD test guideline N° 432 [30]. In brief, 3T3 cells (1×10^4 cells/well) were seeded in two 96-well plates and incubated overnight. After, cells were exposed, for 1 h, to LQFM184 (**2**) (3.1-400 µg/mL), amiodarone HCL (3.1-400 µg/mL) or vehicle controls (0.4% DMSO or 0.1% ethanol for LQFM184 (**2**) or amiodarone HCL, respectively). Subsequently, one plate was exposed to 5 J/cm² UVA (UVA+),

while another one was protected from light (UVA-). After 50-min exposure, cells were washed with HBSS and a fresh medium was added in each well. After 18 h, cells were washed again, and DMEM containing neutral red (50 $\mu\text{g}/\text{mL}$) was added to all wells to evaluate the cell viability as described in item 2.8.2. Absorbance was measured at 540 nm. The Phototox Version 2.0 software, available by OECD, was used to obtain the photoirritation factor (PIF) and mean photo effect (MPE). According to the guideline, a compound can be classified as follows: “No phototoxic” (PIF < 2 or MPE < 0.1); “Probable phototoxic” (2 < PIF < 5 or 0.1 < MPE < 0.15); or “Phototoxic” (PIF > 5 or MPE > 0.15).

Statistical analysis

Three independent assays were performed, and the data analyzed using GraphPad Prism version 5.01 software (San Diego, CA, USA). The one-way Analysis of Variance (ANOVA) followed by Dunnett’s were used for multiple comparisons. Statistical significance was considered as $p < 0.05$.

RESULTS

Synthesis

As shown in Fig. 2, the first step of the synthetic route of LQFM184 (**2**) was the synthesis of 2-(4-hydroxy-3-methoxybenzylidene) malononitrile (**5**) (92 % of yield) through Knoevenagel reaction [13]. In sequence, (*E*)-2-cyano-3-(4-hydroxy-3-methoxyphenyl)acrylamide (**6**) was obtained in 93% of yield through stereoselective copper(II)-catalyzed monohydration of 2-(4-hydroxy-3-methoxybenzylidene) malononitrile (**5**) [14]. The same compound (**6**) also could be synthesized, in 80 % of yield, using neat Knoevenagel conditions [15]. Finally, LQFM184 (**2**) was acquired in 62% of yield through aromatic nucleophilic substitution reaction [16, 17]. In total, it was synthesized in three synthetic steps with global yield of 45-53 %.

<Figure 2>

Stability assessment of LQFM184 (**2**) against oxidation

The DPV method was used to evaluate the anodic behavior and oxidative stability of compounds (**5**), (**6**) and LQFM184 (**2**). In relation to the intermediate compounds, (**5**) and (**6**), the free phenolic group was electrochemically oxidized at glassy carbon electrode, showing an anodic peak, 1a, at peak potential, $E_{p1a} = 0.6$ V (Fig. 3).

On the other hand, it was verified a complete absence of anodic peaks in the DP voltammogram of LQFM184 (**2**), in which all phenolic groups are involved in ether linkages to the central 1,3,5-triazine ring. Therefore, it can be assumed that LQFM184 (**2**) has good stability against oxidation, which is a promising feature for a photoprotective molecule [11].

<Figure 3>

Thermogravimetric curve of LQFM184 (**2**)

Analysis of the thermogravimetric curve suggested that LQFM184 (**2**) is thermally stable up to high temperatures (Fig. 4). To demonstrate this, LQFM184 (**2**) was subjected to heating ramp. We observed, until 100°C approximately, a mild mass loss of about 0.126 mg, representing 2.565% of the original mass. This loss can be attributed to moisture (water) adsorbed onto the structure. After, the

thermal decomposition occurred in three consecutive mass loss steps, as shown in DTG curve of LQFM184 (**2**), while its complete degradation was demonstrated in DTA curve. Despite the fact it was not possible to identify the compounds released by thermal degradation using TG, it is reasonable association with the results of mass spectroscopy. The first step occurred in high temperatures (240-415°C) with weight loss of 30%; this can be given to loss of the one of the three $C_{11}H_7N_2O_2$ molecules found in the LQFM184 (**2**). Then, the second and third decomposition steps happened at 415.43-571.6°C and 571.6-700°C with weight loss of 33.25 and 33.82%, respectively. These values can be assigned to loss of the other two $C_{11}H_7N_2O_2$ molecules with the $C_3N_3O_3$ molecule core.

<Figure 4>

Photophysical characterization of LQFM184 (**2**)

The photophysical characterization of LQFM184 (**2**) is shown in Fig. 5A. The LQFM184 (**2**) showed an intense absorption from 260 to 340 nm (UVA and UVB regions), with a main band at 298 nm and a shoulder close to 334 nm. The molar absorption coefficient ($\epsilon(\lambda)$) was calculated from the absorbance spectra using the Beer-Law $\epsilon(\lambda) = A(\lambda)/Cl$, where $A(\lambda)$ is the absorbance spectra of the solution, C is the molar concentration and l is the optical length of the quartz cell [31, 32]. In a graph of $A(\lambda)$ as a function of C , the slope is $\epsilon(\lambda)l$ (inset of Fig. 5A). In the experiments performed, the LQFM184 (**2**) concentrations were evaluated from 12.5 to 200 μ M and the optical length of the quartz cell employed was 1.0 cm. The $\epsilon(\lambda=298 \text{ nm})$ value obtained at 298 nm is $3.63 \times 10^4 \text{ M}^{-1}\text{cm}^{-1}$, which is the mean value of five independent measurements.

Fig. 5B shows the fluorescence spectra obtained in different excitation wavelengths. It is observed a single broad structureless band centered close to 448 nm, which is independent of excitation. To avoid the inner filter effect, the solutions were prepared and adjusted to ~ 0.05 absorbance at excitation wavelength. The photophysical processes can be explained based on an energy-level diagram, also called Jablonski's diagram (see inset of Fig. 5B), which comprises the singlet ground state (S_0), the singlet excited state (S_1) and the triplet excited states (T_1) [32].

<Figure 5>

SPF evaluation of LQFM184 (2)

The method used in this study was an *in vitro* technique for predicting the effect of compound LQFM184 (2) considering human skin protection from UV radiation exposure. Data from the literature have shown that *in vitro* results have good correlation to those obtained using *in vivo* assays [34]. When LQFM184 (2) was evaluated by Optometrics SPF-290S analyzer, the SPF value found was 2.62. Moreover, its combination with ethylhexyl methoxycinnamate and Tinosorb® S provided SPF values of 20.29 and 26.83, respectively. In addition, a commercial sunscreen with SPF30 showed a SPF value of 31.3, while a value of 35.14 was obtained when LQFM184 (2) was added on this product.

Estimation of the acute oral systemic toxicity hazard for LQFM184 (2)

For acute toxicity profile investigation, we performed the validated *in vitro* 3T3 NRU assay to predict the LD₅₀ of LQFM184 (2). In Fig. 6, it is observed that LQFM184 (2) triggered cytotoxicity in a concentration-dependent manner. IC₅₀ value found was 15.2 µg/mL, which was used to estimate de LD₅₀. Thus, the estimated LD₅₀ value for LQFM184 (2) was 495.4 mg/kg, classifying it as UN GHS Category 4 (LD₅₀ > 300-2000 mg/kg).

<Figure 6>

Eye toxicity assessment of LQFM184 (2)

The eye toxicity profile of LQFM184 (2) was studied using four different endpoints: cytotoxicity to epithelial cells, corneal opacity damage, corneal permeability and histomorphometry. The positive control used, benzalkonium chloride, promoted high cytotoxicity according to the STE assay (Table 2) and then this compound was properly classified as UN GHS Category 1. Corroborating with these findings, the corneal opacity and permeability changes produced an IVIS of 101.95, classifying this compound as Category 1 in BCOP assay (Table 3).

<Table 2 >

<Table 3 >

On the other hand, SIRC cells exposed to LQFM184 (**2**) concentrations at 0.05 and 5% showed a low decrease in cell viability of 86.5 and 72.1%. Therefore, it was classified as non-irritant. Furthermore, BCOP data showed that LQFM184 (**2**) did not promote significant corneal permeability/opacity changes (IVIS value of 6.38), with no potential to predict eye irritation (Table 3). In this respect, corneal histomorphometric assessments were performed to improve the prediction model of the BCOP method [27]. Histomorphometric results showed that LQFM184 (**2**) did not trigger any corneal tissue damages, showing epithelium and stroma lengths of 60.01 and 394.43 μm , respectively, which were similar to those values found for control (51.87 μm for epithelium and 440.59 μm for stroma) (Figs. 7A-C). In contrast, benzalkonium chloride was able to cause a drastic reduction of 35.61 μm ($p < 0.0001$) in corneal epithelium length (Fig. 7A) in parallel to an increase of 597.62 μm ($p < 0.0001$) in stroma length (Fig. 7B).

<Figure 7>

Skin sensitization evaluation of LQFM184 (2**)**

As shown in Fig. 8A, the keratinocyte cells exposed to LQFM184 (**2**) (1.6-200 $\mu\text{g}/\text{mL}$) produced a reduction on cell viability, with an IC_{20} value of 8 $\mu\text{g}/\text{mL}$. At this concentration, the compound was unable to promote an increase in IL-18 intracellular production, when compared to vehicle and control groups, with a reduced SI value of 0.36 (Fig. 8B). In addition, LQFM184 (**2**) did not promote changes in gene expression of *NRF2* and *FOS* (Fig. 8C). Thus, the compound was classified as non-skin sensitizer considering the keratinocyte activation endpoint. It has been demonstrated in the literature that skin sensitizers promote significant increase of IL-18 levels in keratinocytes [28] as well as modulation of the Nrf2-Keap1 pathway and, consequently, the inflammatory response (e.g. *FOS* and *FosLI*) [36]. In contrast, the well-known skin sensitizer PPD triggered a significant increase in IL-18 levels ($p < 0.0001$), with a SI value of 10.04, associated with significant changes in *NRF2* and *FOS* gene expression ($p < 0.001$).

<Figure 8>

Moreover, U937 cells exposed to LQFM184 (**2**) showed reduction on cell viability in a concentration-dependent manner (Fig. 9A), reaching a CV_{70} value of 10 $\mu\text{g/mL}$. These cells were then exposed to LQFM184 (**2**) at non-cytotoxic concentrations (1.25-10 $\mu\text{g/mL}$) to perform U-SENSTM. As shown in Fig. 9B, the skin sensitizer DNCB (1 $\mu\text{g/mL}$) induced a significant increase in CD86 expression (SI=266.17%) ($p<0.001$), in comparison to control. Regarding to LQFM184 (**2**), only the higher concentration (10 $\mu\text{g/mL}$) was able to generate a significant increase in CD86 expression (SI=247.68%) ($p<0.05$). Considering that SI value of CD86 was higher than 150% at the highest non-cytotoxic LQFM184 (**2**) concentration only, no conclusion regarding skin sensitization potential can be made by this parameter.

These results led us to investigate a third endpoint through quantification of IL-8 levels released by U937 cells exposed to LQFM184 (**2**) (1.25-10 $\mu\text{g/mL}$). In the same way as the results observed in the expression of CD86, DNCB (1 $\mu\text{g/mL}$) triggered an increased in IL-8 levels ($p<0.0001$) associated with a high SI value of 5.70, when compared to control. Contrasting, LQFM184 (**2**) did not promote significant increases in IL-8 levels (Fig. 9C).

<Figure 9>

Phototoxicity evaluation of LQFM184 (2)

The results of the phototoxicity investigation of LQFM184 (**2**) are shown in Table 4. The positive control used, amiodarone HCL, was properly classified as a phototoxic substance with PIF and MPE values of 8.30 and 0.43, respectively. On the other hand, LQFM184 (**2**) was classified as potentially non-phototoxic. The IC_{50} values found were 43.32 $\mu\text{g/mL}$ (UVA- exposure) and 32.71 $\mu\text{g/mL}$ (UVA+ exposure), whereas PIF and MPE values of 1.32 and 0.05, respectively.

<Table 4 >

DISCUSSION

LQFM184 (**2**) was designed through bioisosterism of functional group strategy from LQFM048 (**1**). The amide scaffold found in LQFM184 (**2**) can add the possible advantage to form hydrogen bonds with sunscreen formulations as well as skin, when compared to the lead compound. The synthetic

route used allowed LQFM184 (**2**) be synthesized only in three synthetic steps, with around 45-53 % of global yield.

Evaluations of the physico-chemical properties of the new compound LQFM184 (**2**), using the TG, DTG and DTA methodologies, showed steady against temperature escalations, with a stable structure for possible use in sunscreens [11]. Considering that, LQFM184 (**2**) degradation may start at much higher values than the maximum values of handling, manipulation and manufacture of finished product (around 80 °C), as well as, the use of the finished product (about 50 °C).

The photophysical characterization demonstrated that LQFM184 (**2**), similarly to typical commercial sunscreen, possesses ϵ from 10^3 - 10^5 M⁻¹cm⁻¹ in the UVA and UVB regions. As shown before, the photophysical data obtained with the evaluation of the LQFM184 (**2**) can be explained based on an energy-level diagram, also called Jablonski's diagram, which comprises the singlet ground state (S₀), the singlet excited state (S₁) and the triplet excited states (T₁) [32]. In thermodynamic equilibrium, the molecules lying in the lowest electronic state S₀ can reach excited state S₁, due to one photon absorption, described by molar absorption coefficient $\epsilon(\lambda)$ (see inset of Fig. 5B). At S₁ state, the molecules can lose energy in a variety of different ways: (i) decaying to S₀ through a radiative process described by a rate constant k_R ; (ii) decaying to S₀ through an internal conversion process (k_{IC}); or (iii) decaying to the triplet state T₁ by an intersystem crossing process (k_{ISC}) [32]. While the radiative process is linked to the fluorescence of the molecules by photons emission, the internal conversion and the intersystem crossing processes can produce heat to the environment. Aiming at the potential application of LQFM184 (**2**) in sun protection products, the intense fluorescence observed here can be a strategy to produce less heat in a future formulation. In order to obtain an efficient sunscreen formulation, high Stokes shifts ($\Delta\nu = \nu_{\text{abs}} - \nu_{\text{em}}$) are desired [12]. High Stokes shifts values mean a more efficient separation between absorption in the UV region (ν_{abs}) and energy released as the light emitted in the visible region (ν_{em}).

Similarly to its lead compound LQFM048 (**1**) [12], the SPF values obtained for LQFM184 (**2**) suggest that its association with other filters present in a formulation can increase the SPF value. The degree to which this increase in SPF occurs is different for each filter, possibly by different modes of molecular interaction between filters and the new product tested. Thus, it seems to be interesting

associate LQFM184 (2) with other sunscreens, since it promotes slightly higher protective factors without the need to incorporate more commercial filters, which have limits set by current Brazilian legislation, for instance.

The acute toxicity profile is important for identifying and characterizing hazard induced by chemical [35]. In this context, we estimated the LD₅₀ value for LQFM184 (2) as 495.4 mg/kg using a validated *in vitro* model the 3T3 NRU assay, categorizing it in UN GHS category 4 (LD₅₀ > 300-2000 mg/kg). Regarding eye toxicity, the data obtained using three different endpoints indicated that LQFM184 (2) does not promote potential eye toxicity.

Concerning the potential of LQFM184 (2) to induce skin allergy, the compound was classified as non-skin sensitizer by combined analysis of different *in vitro* innovative methodologies for skin sensitizing prediction [37]. Moreover, the results of the phototoxicity investigation of LQFM184 (2) showed that it is potentially non-phototoxic, corroborating with all efficacy/toxicity data presented here and suggesting its promising use as a sunscreen ingredient due to its UV filter properties.

The novel photoprotective compound LQFM184 (2), synthesized by green chemistry approach, was stable under oxidative/high-temperature conditions, showed good efficacy covering a wide UV range, from 260 to 340 (UVA and UVB regions). Toxicological investigations showed that compound (2) has a low-moderate potential of inducing acute oral systemic toxicity hazard. In addition, eye irritation, skin sensitization and phototoxic potential effects were not observed for LQFM184 (2). These findings make LQFM184 (2) a promising agent to be used in cosmetic products such as sunscreens.

ACKNOWLEDGEMENTS: This work was supported by Fundação de Apoio à Pesquisa do Estado de Goiás (FAPEG), Conselho Nacional de Desenvolvimento Científico e Tecnológico (CNPq) and Coordenação de Aperfeiçoamento de Pessoal de Nível Superior (CAPES) (finance code 001).

SUPPORTING INFORMATION

Additional supporting information may be found online in the Supporting Information section at the end of the article:

Table S1. ^1H and ^{13}C NMR spectral data for 2-cyano-3-(4'-hydroxy-3'-methoxybenzylidene)-malononitrile (**5**) in DMSO- d_6 .

Table S2. ^1H and ^{13}C NMR spectral data for (*E*)-2-cyano-3-(4-hydroxy-3-methoxyphenyl)-acrylamide (**6**) in DMSO- d_6 .

Table S3. ^1H and ^{13}C NMR spectral data for (2,4,6-tris-((*E*)-2-cyano-3-(4-hydroxy-3-methoxyphenyl)acrylamide)-1,3,5-triazine) (**2**), in DMSO- d_6 .

Figure S1. Infrared spectrum obtained for 2-cyano-3-(4'-hydroxy-3'-ethoxybenzylidene)-malononitrile (**5**).

Figure S2. ^1H NMR spectrum obtained for 2-cyano-3-(4'-hydroxy-3'-methoxybenzylidene)-malononitrile (**5**) in DMSO- d_6 .

Figure S3. HSQC contour map for 2-cyano-3-(4'-hydroxy-3'-methoxybenzylidene)-malononitrile (**5**) in DMSO- d_6 .

Figure S4. HMBC contour map for 2-cyano-3-(4'-hydroxy-3'-methoxybenzylidene)-malononitrile (**5**) in DMSO- d_6 .

Figure S5. ESI (-) FT-Orbitrap MS spectrum obtained for 2-cyano-3-(4'-hydroxy-3'-methoxybenzylidene)-malononitrile (**5**).

Figure S6. Infrared spectra obtained for (*E*)-2-cyano-3-(4-hydroxy-3-methoxyphenyl)-acrylamide (**6**).

Figure S7. ^1H NMR spectrum for (*E*)-2-cyano-3-(4-hydroxy-3-methoxyphenyl)-acrylamide (**6**), in DMSO- d_6 .

Figure S8. HSQC contour map for (*E*)-2-cyano-3-(4-hydroxy-3-methoxyphenyl)-acrylamide (**6**), in DMSO- d_6 .

Figure S9. HMBC contour map for (E)-2-cyano-3-(4-hydroxy-3-methoxyphenyl)-acrylamide (**6**), in DMSO-d₆.

Figure S10. ESI (-) FT-Orbitrap MS spectra obtained for (E)-2-cyano-3-(4-hydroxy-3-methoxyphenyl)-acrylamide (**6**).

Figure S11. Infrared spectrum obtained for (2,4,6-tris-((E)-2-cyano-3-(4-hydroxy-3-methoxyphenyl)acrylamide)-1,3,5-triazine) (**2**) – LQFM184.

Figure S12. ¹H NMR spectrum obtained for (2,4,6-tris-((E)-2-cyano-3-(4-hydroxy-3-methoxyphenyl)acrylamide)-1,3,5-triazine) (**2**), in DMSO-d₆.

Figure S13. HSQC contour map for (2,4,6-tris-((E)-2-cyano-3-(4-hydroxy-3-methoxyphenyl)acrylamide)-1,3,5-triazine) (**2**), in DMSO-d₆.

Figure S14. HMBC contour map for (2,4,6-tris-((E)-2-cyano-3-(4-hydroxy-3-methoxyphenyl)acrylamide)-1,3,5-triazine) (**2**), in DMSO-d₆.

Figure S15. ¹³C NMR spectrum obtained for (2,4,6-tris-((E)-2-cyano-3-(4-hydroxy-3-methoxyphenyl)acrylamide)-1,3,5-triazine) (**9**), in DMSO-d₆.

Figure S16. ESI (+) FT-Orbitrap MS spectra obtained for (2,4,6-tris-((E)-2-cyano-3-(4-hydroxy-3-methoxyphenyl)acrylamide)-1,3,5-triazine) (**9**).

REFERENCES

- [1] J.A. Ruszkiewicz, A. Pinkas, B. Ferrer, T.V. Peres, A. Tsatsakis, M. Aschner, Neurotoxic effect of active ingredients in sunscreen products, a contemporary review, *Toxicol Rep*, 4 (2017) 245-259.
- [2] M.S. Latha, J. Martis, V. Shobha, R. Sham Shinde, S. Bangera, B. Krishnankutty, S. Bellary, S. Varughese, P. Rao, B.R. Naveen Kumar, Sunscreening agents: a review, *J Clin Aesthet Dermatol*, 6 (2013) 16-26.
- [3] A. Sample, Y.-Y. He, Mechanisms and prevention of UV-induced melanoma, *Photodermatol Photoimmunol Photomed*, 34 (2018) 13-24.
- [4] V. Fioletov, J.B. Kerr, A. Fergusson, The UV index: definition, distribution and factors affecting it, *Can J Public Health*, 101 (2010) I5-9.
- [5] S. Deady, L. Sharp, H. Comber, Increasing skin cancer incidence in young, affluent, urban populations: a challenge for prevention, *Br J Dermatol*, 171 (2014) 324-331.
- [6] Q. Zhang, X. Ma, M. Dzakpasu, X.C. Wang, Evaluation of ecotoxicological effects of benzophenone UV filters: luminescent bacteria toxicity, genotoxicity and hormonal activity, *Ecotoxicol Environ Saf*, 142 (2017) 338-347.
- [7] F. Vela-Soria, I. Jiménez-Díaz, R. Rodríguez-Gómez, A. Zafra-Gómez, O. Ballesteros, A. Navalón, J.L. Vilchez, M.F. Fernández, N. Olea, Determination of benzophenones in human placental tissue samples by liquid chromatography–tandem mass spectrometry, *Talanta*, 85 (2011) 1848-1855.
- [8] B. Herzog, D. Hüglin, E. Borsos, A. Stehlin, H. Luther, New UV absorbers for cosmetic sunscreens – a breakthrough for the photoprotection of human skin, *Chimia*, 58 (2004) 554-559.
- [9] S.Q. Wang, P.R. Tanner, H.W. Lim, J.F. Nash, The evolution of sunscreen products in the United States – a 12-year cross sectional study, *Photochem Photobiol Sci*, 12 (2013) 197-202.
- [10] C. Couteau, E. Papis, C. Chauvet, L. Coiffard, Tris-biphenyl triazine, a new ultraviolet filter studied in terms of photoprotective efficacy, *Int J Pharm*, 487 (2015) 120-123.
- [11] D. Hüglin, Advanced UV absorbers for the protection of human skin, *Chimia*, 70 (2016) 496-501.

- [12] D.C. Vinhal, R.I. de Ávila, M.S. Vieira, R.M. Luzin, M.P. Quintino, L.M. Nunes, A.C.C. Ribeiro, H.S. de Camargo, A.C. Pinto, H.M. dos Santos Júnior, B.G. Chiari, V. Isaac, M.C. Valadares, T.D. Martins, L.M. Lião, E. de S. Gil, R. Menegatti, Photoprotective effect and acute oral systemic toxicity evaluation of the novel heterocyclic compound LQFM048, *J Photochem Photobiol B*, 161 (2016) 50-58.
- [13] R.I. de Ávila, M. de Sousa Vieira, M.P.N. Gaeti, L.C. Moreira, L. de Brito Rodrigues, G.A.R. de Oliveira, A.C. Batista, D.C. Vinhal, R. Menegatti, M.C. Valadares, Toxicity evaluation of the photoprotective compound LQFM048: eye irritation, skin toxicity and genotoxic endpoints, *Toxicology*, 376 (2017) 83-93. [13] M.N. Gomes, C.M.A. de Oliveira, C.F.D. Garrote, V. de Oliveira, R. Menegatti, Condensation of Ethyl Cyanoacetate with Aromatic Aldehydes in Water, Catalyzed by Morpholine, *Synth Commun*, 41 (2010) 52-57.
- [14] X. Xin, D. Xiang, J. Yang, Q. Zhang, F. Zhou, D. Dong, Homogeneous and stereoselective copper(II)-catalyzed monohydration of methylenemalononitriles to 2-cyanoacrylamides, *J Org Chem*, 78 (2013) 11956-11961.
- [15] K. Lewellyn, D. Bialonska, N.D. Chaurasiya, B.L. Tekwani, J.K. Zjawiony, Synthesis and evaluation of aplysinopsin analogs as inhibitors of human monoamine oxidase A and B, *Bioorg Med Chem Lett*, 22 (2012) 4926-4929.
- [16] R. Menicagli, S. Samaritani, G. Signore, F. Vaglini, L. Dalla Via, *In vitro* cytotoxic activities of 2-alkyl-4,6-diheteroalkyl-1,3,5-triazines: new molecules in anticancer research, *J Med Chem*, 47 (2004) 4649-4652.
- [17] H. Duan, L. Wang, D. Qin, X. Li, S. Wang, Y. Zhang, Synthesis and characterization of some new star-shaped polydentate ligands from 2,4,6-trichloro-1,3,5-triazine, *Synth Commun*, 41 (2011) 380-384.
- [18] M.A. Corrêa, *Cosmetologia*, in, Medfarma, 2012, pp. 492.
- [19] S. Kale, P. Ghoge, A. Ansari, A. Waje, A. Sonawane, Formulation and *in-vitro* determination of sun protection factor of *Nigella sativa* Linn. seed oil sunscreen cream, *Int J Pharm Tech Res*, 2 (2010) 2194-2197.
- [20] A. Duraisamy, N. Narayanaswamy, A. Sebastian, K.P. Balakrishnan, Sun protection and anti-inflammatory activities of some medicinal plants, *Int J Res Cosm Sci*, 1 (2011) 13-16.

- [21] E. Borenfreund, J.A. Puerner, A simple quantitative procedure using monolayer cultures for cytotoxicity assays (HTD/NR-90), *J Tissue Cult Methods*, 9 (1985) 7-9.
- [22] ICCVAM, Test method evaluation report (TIMER): *in vitro* cytotoxicity test methods for estimating starting doses for acute oral systemic toxicity test. NIH publication no. 07-4519. Research Triangle Park, NC: National Institute for Environmental Health Sciences, (2006).
- [23] M.d.S. Vieira, V. de Oliveira, E.M. Lima, M.J. Kato, M.C. Valadares, *In vitro* basal cytotoxicity assay applied to estimate acute oral systemic toxicity of grandisin and its major metabolite, *Exp Toxicol Pathol*, 63 (2011) 505-510.
- [24] OECD, Test No. 423: acute oral toxicity - acute toxic class method, 2002.
- [25] OECD, Test No. 442E: *In vitro* skin sensitisation assays addressing the key event on activation of dendritic cells on the adverse outcome pathway for skin sensitisation, OECD Publishing, 2018.
- [26] OECD, Test No. 437: bovine corneal opacity and permeability test method for identifying i) chemicals inducing serious eye damage and ii) chemicals not requiring classification for eye irritation or serious eye damage, 2017.
- [27] G.A.R. Oliveira, R.d.N. Ducas, G.C. Teixeira, A.C. Batista, D.P. Oliveira, M.C. Valadares, Short time exposure (STE) test in conjunction with bovine corneal opacity and permeability (BCOP) assay including histopathology to evaluate correspondence with the Globally Harmonized System (GHS) eye irritation classification of textile dyes, *Toxicol In Vitro*, 29 (2015) 1283-1288.
- [28] E. Corsini, V. Galbiati, M. Mitjans, C.L. Galli, M. Marinovich, NCTC 2544 and IL-18 production: a tool for the identification of contact allergens, *Toxicol In Vitro*, 27 (2013) 1127-1134.
- [29] OECD, Test No. 442E: *in vitro* skin sensitisation, 2018.
- [30] OECD, Test No. 432: *in vitro* 3T3 NRU phototoxicity test, 2004.
- [31] S.E. Rodrigues, A.E.H. Machado, M. Berardi, A.S. Ito, L.M. Almeida, M.J. Santana, L.M. Liao, N.M. Barbosa Neto, P.J. Gonçalves, Investigation of protonation effects on the electronic and structural properties of halogenated sulfonated porphyrins, *J Mol Struct*, 1084 (2015) 284-293.
- [32] L. Alonso, R.N. Sampaio, T.F.M. Souza, R.C. Silva, N.M.B. Neto, A.O. Ribeiro, A. Alonso, P.J. Gonçalves, Photodynamic evaluation of tetracarboxy-phthalocyanines in model systems, *J Photochem Photobiol B*, 161 (2016) 100-107.

[33] C. Couteau, M. Pommier, E. Papis, L. Coiffard, Study of the efficacy of 18 sun filters authorized in European Union tested *in vitro*, *Pharmazie*, 62 (2007) 449-452.

[34] P.J. Matts, V. Alard, M.W. Brown, L. Ferrero, H. Gers-Barlag, N. Issachar, D. Moyal, R. Wolber, The COLIPA *in vitro* UVA method: a standard and reproducible measure of sunscreen UVA protection, *Int J Cosmet Sci*, 32 (2010) 35-46.

[35] ICCVAM, Guidance document on using *in vitro* data to estimate *in vivo* starting doses for acute toxicity. NIH Publication no. 01-4500. Research Triangle Park, NC: National Institute for Environmental Health Sciences., (2001).

[36] J.W. van der Veen, T.E. Pronk, H. van Loveren, J. Ezendam, Applicability of a keratinocyte gene signature to predict skin sensitizing potential, *Toxicol In Vitro*, 27 (2013) 314-322.

[37] C. Bauch, S.N. Kolle, T. Ramirez, T. Eltze, E. Fabian, A. Mehling, W. Teubner, B. van Ravenzwaay, R. Landsiedel, Putting the parts together: combining *in vitro* methods to test for skin sensitizing potentials, *Regul Toxicol Pharmacol*, 63 (2012) 489-504.

FIGURE CAPTIONS

Figure 1. Design of LQFM184 (2) from LQFM048 (1) lead compound.

Figure 2. Synthetic route of LQFM184 (2).

Figure 3. DP voltammograms obtained for 10 μ M solutions of LQFM184 (2) (●●●), compound (5) (—) and compound (6) (- - -) in phosphate buffer saline (pH 6.0 0.1 M).

Figure 4. Representative thermogravimetric analysis of LQFM184 (2).

Figure 5. Photophysical characterization of LQFM184 (2). (A) Absorption spectra of LQFM184 (2) in DMSO and in different concentrations, *inset*: $A(\lambda)$ vs C curve. (B) Fluorescence spectra of LQFM184 (2) at different excitation wavelengths, *inset*: energy-level diagram (Jablonski's diagram).

Figure 6. Cytotoxicity analysis of LQFM184 (**2**) in 3T3 fibroblasts. Cells (0.5×10^5 cells/mL) were seeded in plates overnight and then exposed to LQFM184 (**2**) (1.6-200 $\mu\text{g/mL}$). After 48 h incubation, the cell viability was evaluated by neural red uptake (NRU) assay. The IC_{50} value (15.2 $\mu\text{g/mL}$) obtained was used to estimate LD_{50} of LQFM 184 (**2**).

Figure 7. Corneal histomorphometric analysis. Isolated corneas ($n=3/\text{group}$) from bovine eyes were exposed to LQFM184 (**2**) (5%), its vehicle (2.5% DMSO), negative (PBS) and positive (benzalkonium chloride at 5%) controls. After that, the samples were processed, and tissue sections obtained and stained with hematoxylin and eosin (H&E). Histomorphometric assessment was carried out through measurement of thickness of the (A) epithelium and (B) stroma. (C) Representative photomicrographs of corneas exposed to PBS and LQFM184 (**2**) ($10 \times$ magnification).

Figure 8. HaCaT keratinocytes-associated IL-18 assay. (A) HaCaT cells (1.5×10^5 cells/mL) were seeded in plates overnight and then exposed to LQFM184 (**2**) (1.6-200 $\mu\text{g/mL}$) for 24 h. The cell viability was analyzed by MTT assay. (B) Cells were exposed to non-cytotoxic concentration of LQFM184 (**2**) ($\text{IC}_{20} = 8 \mu\text{g/mL}$), the skin sensitizer PPD (40 $\mu\text{g/mL}$), vehicle control (0.4% DMSO) or complete medium only (control cells). After 24 h exposure, IL-18 levels were quantified in cell lysates. Data represent the mean \pm SD of three independent experiments. (***) $p < 0.0001$ vs. control or DMSO (0.4%). ANOVA followed by Dunnett's test).

Figure 9. U937 cell line activation test (U-SENSTM) and IL-8 levels analysis. (A) U937 cells (5×10^5 cells/mL) were exposed to LQFM184 (**2**) (1.6-200 $\mu\text{g/mL}$) for 24 h. After that, cell viability was analyzed by propidium iodide staining using flow cytometer. (B) U937 cells were exposed to non-cytotoxic concentrations of LQFM184 (**2**) (1.25-10 $\mu\text{g/mL}$), the skin sensitizer DNCB (1 $\mu\text{g/mL}$), vehicle control (0.4% DMSO) or complete medium only (control group) for 45 h. CD86 analysis was then conducted by flow cytometry. (C) IL-8 levels found in supernatant of U937 cells.

Tables**Table 1.** PCR primer sequences and associated GenBank accession numbers.

Gene	Name	Primer sequence (5' – 3')	GenBank number
<i>NRF2</i>	Nuclear factor, erythroid 2 like 2	AGT GGA TCT GCC AAC TAC TC CAT CTA CAA ACG GGA ATG TCT G	S74017.1
<i>FOS</i>	Fos proto-oncogene	TGC CTC TCC TCA ATG ACC CTG A ATA GGT CCA TGT CTG GCA CGG A	CR542267.1
<i>HPRT1</i>	Hypoxanthine phosphoribosyltransferase 1	TGA CAC TGG CAA AAC AAT GAC GGT CCT TTT CAC CAG CAA GCT	CR407645.1

Table 2. Data obtained in the short time exposure (STE) assay.

Exposure group	Cell viability (%)		UN GHS classification ^b
	0.05%	5%	
Negative control ^a	100 ± 0.5	100 ± 0.3	No category
Positive control ^a	5.6 ± 1.1	2.7 ± 0.5	Category 1
LQFM184 (2)	86.5 ± 0.8	72.1 ± 0.3	No category

Data represent mean ± SD of three independent assays.

^aSaline and benzalkonium chloride are negative and positive controls, respectively.

^bPrediction model based on OECD test guideline N° 491 (OECD, 2015).

Table 3. Data obtained in the bovine corneal opacity and permeability (BCOP) assay.

Exposure group	Opacity	Permeability	IVIS	UN GHS classification ^b
Negative control ^a	0.43 ± 0.31	0.06 ± 0.02	1.33	No category
Positive control ^a	74.80 ± 1.20	1.81 ± 0.54	101.95	Category 1
DMSO (2.5%)	1.0 ± 0.67	0.08 ± 0.01	2.20	No category
LQFM184 (2) (5%)	5.33 ± 0.44	0.07 ± 0.03	6.38	No prediction can be made

Data represent mean or mean ± SD of three independent assays.

^aPBS and benzalkonium chloride are negative and positive controls, respectively.

^bPrediction model based on OECD test guideline N° 437 (OECD, 2013).

Abbreviation: IVIS, *In vitro* irritancy scores.

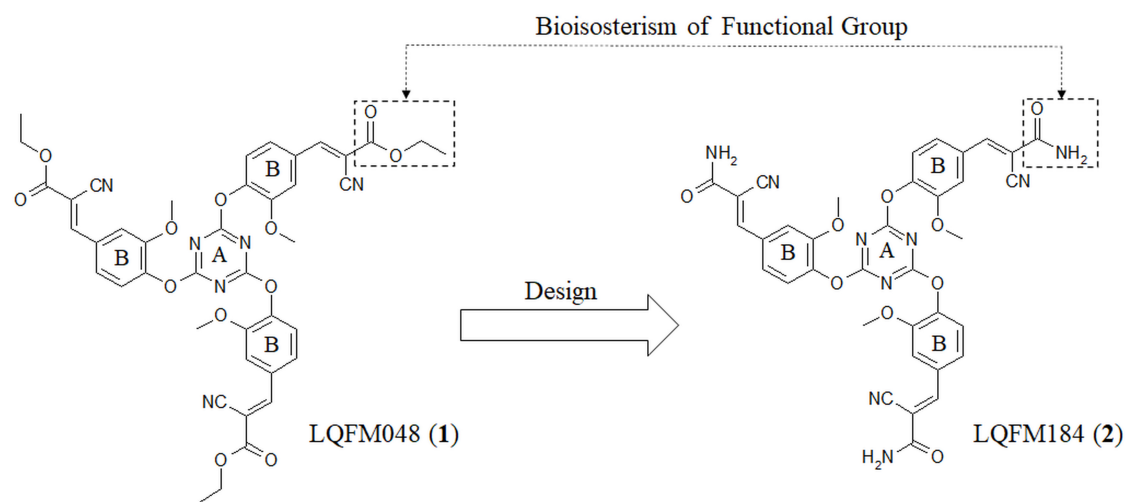
Table 4. Data obtained in the 3T3 neutral red uptake phototoxicity assay.

Exposure group	IC ₅₀ (µg/mL)		PIF	MPE	Classification ^a
	UVA-	UVA+			
Amiodarone HCL	43.86	5.28	8.30	0.43	+
LQFM184 (2)	43.32	32.71	1.32	0.05	-

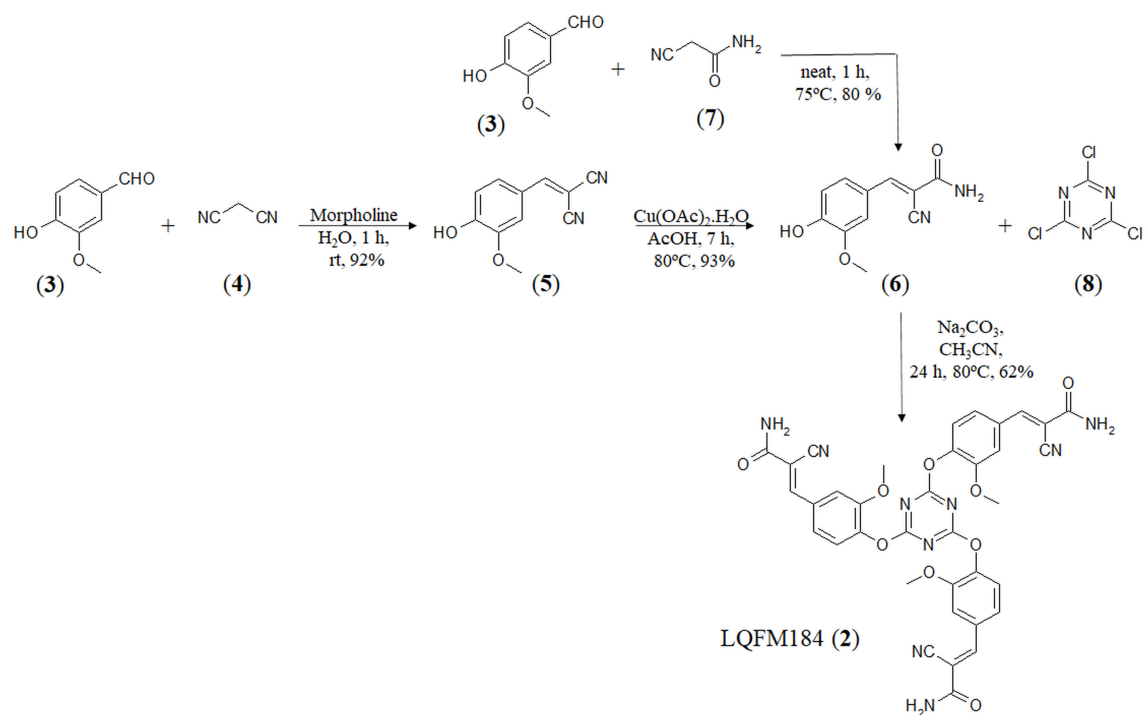
Data represent mean of three independent assays.

^aPrediction model based on OECD test guideline N° 432 (OECD, 2004).

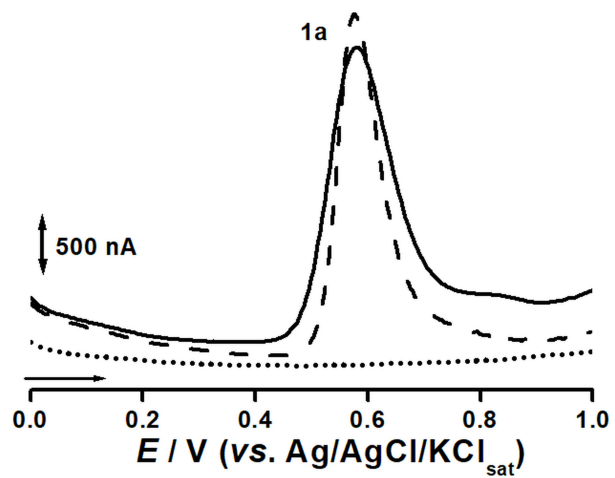
Abbreviations: IC₅₀, concentration that inhibited cell growth by 50% compared to untreated group; PIF, photoirritation factor; MPE, mean photo effect; +, potentially phototoxic substance; -, potentially non-phototoxic substance.



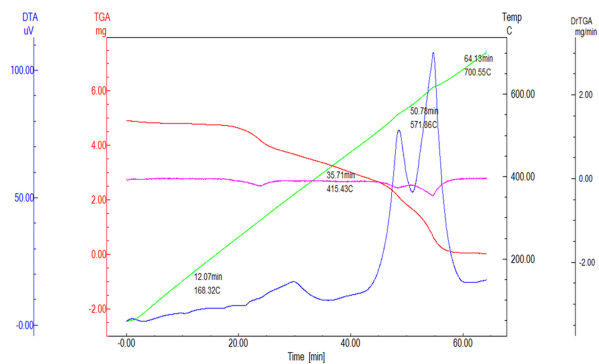
php_13349_f1.jpg



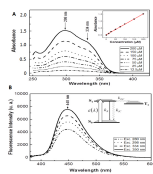
php_13349_f2.jpg



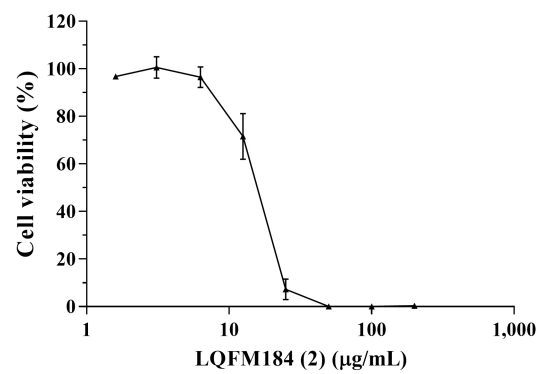
php_13349_f3.jpg



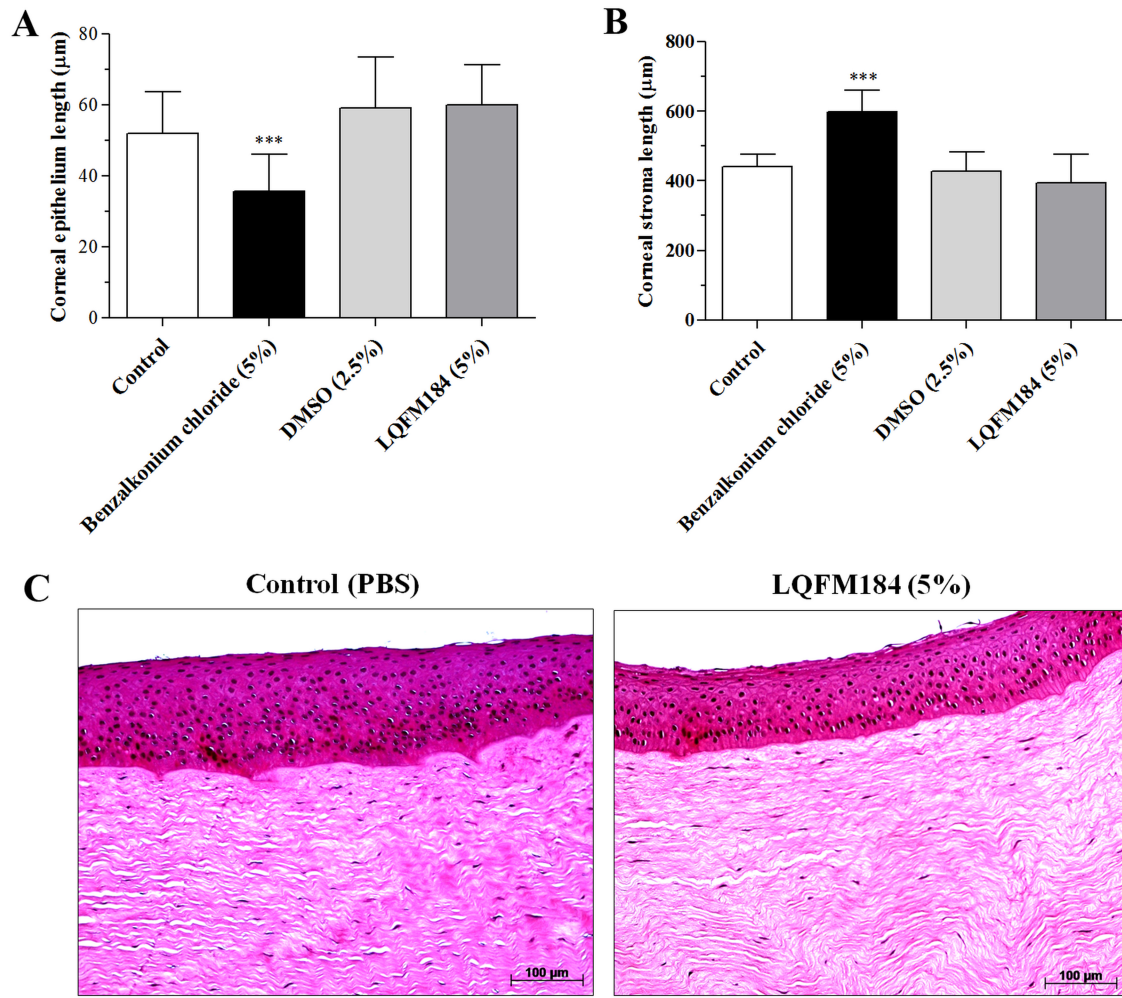
php_13349_f4.jpg



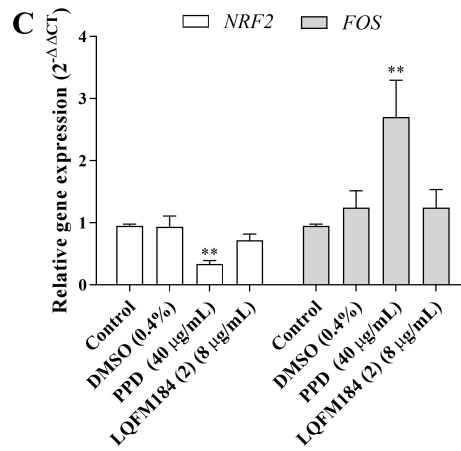
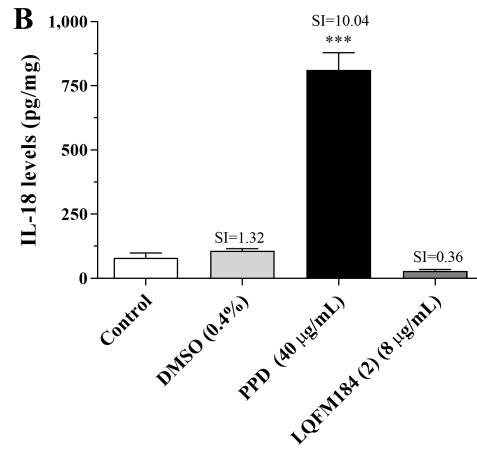
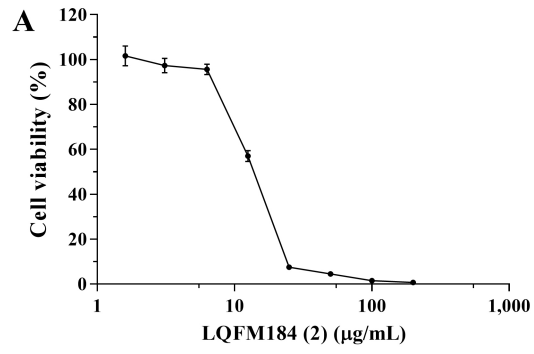
php_13349_f5.jpg



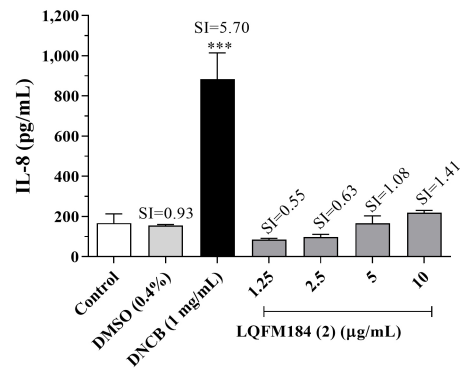
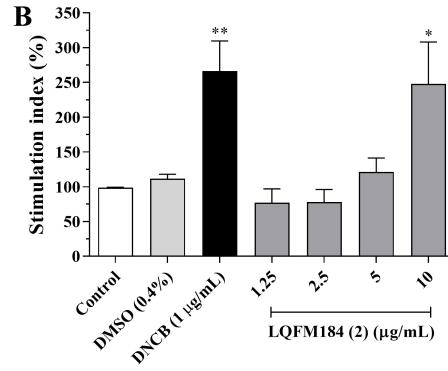
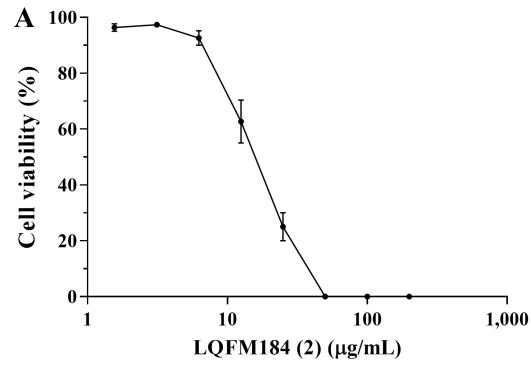
php_13349_f6.jpg



php_13349_f7.jpg



php_13349_f8.jpg



php_13349_f9.jpg